Multi-scale observation of two polar cap arcs occurring on different magnetic field topologies

J. A. Reidy[1,2], R. C. Fear[1], D. K. Whiter [1], B. S. Lanchester[1], A. J. Kavanagh[2], D. J. Price[1], J. M. Chadney[1], Y. Zhang[3]and L. J. Paxton[3]

[1]Department of Physics and Astronomy, University of Southampton, Southampton, UK
[2]British Antarctic Survey, Natural Environment Research Council, Cambridge, UK
[3]The Johns Hopkins University Applied Physics Laboratory, Laurel, MD, USA

Key Points:

- We compare observations (at multiple scales) of two polar cap arcs that are consistent with different formation mechanisms.
- Small-scale observations of polar cap arcs down to scale sizes of meters and temporal resolution of milliseconds are presented.
- Small-scale structures associated with the polar cap arcs in each event are found to be very different, consistent with the two different formation mechanisms.

Corresponding author: Jade Reidy, jadeid70@bas.ac.uk

Abstract

This paper presents observations of polar cap arc substructure down to scale sizes of metres and temporal resolution of milliseconds. Two case studies containing polar cap arcs occurring over Svalbard are investigated. The first occurred on 4 February 2016 and is consistent with formation on closed field lines; the second occurred on 15 December 2015 and is consistent with formation on open field lines. These events were identified using global scale images from the Special Sensor Ultra-violet Spectrographic Imager (SSUSI) instruments on board Defense Meteorological Satellite Program (DMSP) spacecraft. Intervals when the arcs passed through the small scale field of view of the Auroral Structure and Kinetics (ASK) instrument, located on Svalbard, were then found using all sky images from a camera also located on Svalbard. These observations give unprecedented insight into small scale polar cap arc structure. The energy and flux of the precipitating particles above these arcs are estimated using the ASK observations in conjunction with the Southampton Ionospheric model. These estimates are then compared to in-situ DMSP particle measurements, as well as data from ground-based instrumentation, to infer further information about their formation mechanisms. This paper finds that polar cap arcs formed on different magnetic field topologies exhibit different behaviour at small-scale sizes, consistent with their respective formation mechanisms.

1 Introduction

Polar cap arcs occur at high latitudes in the typically dim polar cap region. They are correlated with quiet magnetospheric conditions and northward IMF (Berkey et al., 1976; Gussenhoven et al., 1984). Since polar cap arcs were first discovered, there has been much debate about their formation mechanism. It has been suggested that they occur on either the open field lines of the polar cap (Hardy et al., 1982), the contracted field lines on the edge of the auroral oval (therefore not technically occurring in the polar cap) (Meng, 1981), or on closed field lines which have protruded into the polar cap (Frank et al., 1982).

Large-scale polar cap arcs, such as the theta aurora discovered by Frank et al. (1982), have been found to be associated with particle precipitation of the same energy and brightness as that seen over the auroral oval. Such precipitation, including both ion and electron signatures, has been recorded by many authors when investigating polar cap aurora using high-altitude spacecraft images, for example Frank et al. (1982) and Fear et

al. (2014). This kind of precipitation is consistent with closed field lines and is expected to be seen in both hemispheres simultaneously (e.g. Craven et al. (1991); Carter et al. (2017) and Xing et al. (2018)). There are several theories to explain the existence of closed field lines within the otherwise 'open' polar cap. One theory proposed by Milan et al. (2005) involves the closure of flux in the tail under northward IMF conditions with a strong IMF B_y component. This newly closed flux becomes 'stuck' in the magnetotail and protrudes into the polar cap. Predictions from this mechanism have been confirmed statistically (Fear & Milan, 2012a, 2012b) and through several case studies (e.g. Goudarzi et al. (2008); Fear et al. (2014) and Carter et al. (2017)).

Carlson and Cowley (2005) suggest that weaker polar cap arcs viewed from the ground are distinct from the larger-scale arcs viewed from space and are driven by a different formation mechanism. They state that any modest mechanism which can drive shear flow across open field lines could accelerate polar rain to high enough energies to produce polar cap aurora on these open field lines. The authors expect this type of polar rain aurora, which may be too weak to be picked out by the high-altitude UV imagers, to be present anytime the IMF is northward (which is the case approximately half the time). In their review paper, Newell et al. (2009) argue that these accelerated polar rain arcs may be identified in particle data by an electron-only signature.

It is important to understand auroral structure at all scales, particularly as the small scale processes often affect the bulk properties of a plasma. Relatively little has been done to explore polar cap aurora on very small scales (less than 20 km). Reidy et al. (2017) presented observations from the Auroral Structure and Kinetics (ASK) instrument of a polar cap arc consistent with closed field lines that did not cross the entire polar cap (termed a 'failed' transpolar arc). The ASK instrument, located on Svalbard, is capable of measuring auroral structure down to spatial scales of meters and temporal scales of 0.05 seconds and has generally been used to make observations of the aurora within the main oval (e.g (Lanchester et al., 2009)). Using ASK, Dahlgren et al. (2010) observed boundary undulations (or as they term them, auroral 'ruffs') on the edge of an auroral arc, with amplitudes of less that 800 m. These 'ruffs' demonstrated a much more complex and intricate auroral structure than previously seen before.

This paper will investigate the small scale structure associated with two separate polar cap arc events consistent with different magnetic field topologies, using ASK data.

The multi-scale instrumentation used to investigate the different events is described in section 2. An outline of the methodology used to estimate the energy and energy flux of the precipitation for both events by comparing the ASK observations with an ionospheric model is described in section 2.1.1. The two events are initially discussed separately in sections 3.1 and 3.2 before being compared to one another and to the global scale spacecraft observations in section 4. A conclusion is given in section 5.

2 Instrumentation

2.1 Optical instruments

Global scale images from the Special Sensor Ultra-violet Spectrographic Imager (SSUSI) on board four of the Defense Meteorological Satellite Program (DMSP) spacecraft were used to identify polar cap aurora over Svalbard. SSUSI is an UV imager that scans across the polar regions building up images over approximately 20 minutes; these images are available in 5 different wavelengths simultaneously (Paxton et al., 2002). In this study we use the Lyman Birge Hopfield long band (165-180 nm) which is comparable to wavelengths measured by IMAGE WIC which have been used in previous polar cap arc studies (e.g Fear and Milan (2012a)). The DMSP spacecraft are in sun-synchronous orbits with a period of approximately 90 minutes. This relatively quick orbit means near simultaneous images (separated by approximately 45 minutes) from the northern and southern hemisphere may be obtained from SSUSI. Furthermore, the DMSP spacecraft orbit at around 840 km, which allows SSUSI to observe more fine structure than previous UV imagers, such as Polar UV and IMAGE WIC which orbit at much higher altitudes (see Figure 5 in Fear (2019)).

Images from the Sony a7s camera, located on Svalbard near to the ASK instrument, are used to give the context for the ASK observations. The Sony camera has a circular Fisheye lens with a 180° field of view.

The Auroral Structure and Kinetics (ASK) instrument consists of three cameras with a 6° field of view centred on magnetic zenith (Dahlgren et al., 2008, 2016). Each camera is fitted with a different filter corresponding to specific auroral emissions used in the study of small scale aurora (known as ASK1, ASK2 and ASK3). This paper uses data from the ASK1 and ASK3 cameras. The ASK1 filter is sensitive to the N_2 first positive emission at 632.0 nm; this emission is caused by high energy precipitation. The ASK3

filter is sensitive to the atomic oxygen emission at 777.4 nm, which is caused by both high and low energy precipitation. The ratio of the ASK3/ASK1 emissions provides the characteristics of the precipitation which is then compared to the Southampton Ionospheric model (outlined below in Section 2.1.1) to estimate the energy of precipitating particles (Lanchester et al., 2009). An estimate of the energy flux can be obtained by dividing the brightness measured by ASK1 by the mean modelled brightness within the energy range of each event. This method of estimating the energy and flux has been used in many studies and has been verified by comparison with other ground based instruments, for example the European Incoherent Scatter (EISCAT) radars, (e.g. Lanchester et al. (2009); Whiter et al. (2010); Dahlgren et al. (2011, 2016); Reidy et al. (2017)).

Data from the High Throughput Imaging Echelle Spectrograph (HiTIES) instrument (Chakrabarti et al., 2001), located on Svalbard, have also been obtained for both events. The HiTIES instrument includes an EMCCD detector and a mosaic filter, which is used to record multiple non-contiguous wavelength regions at high resolution. This paper uses data from the 'H-α' panel of a three panel mosaic (installed in December 2015), which observes the wavelength region between 649-663 nm. Doppler shifted hydrogen emissions are a signature of proton precipitation (e.g. Eather (1967)) and are used in this paper to determine the presence of ion precipitation (or lack thereof).

2.1.1 The Southampton Ionospheric model

The Southampton Ionospheric model is an electron transport model (Lummerzheim & Lilensten, 1994) which assumes a neutral atmosphere taken from the MSIS E-90 thermospheric model (Hedin, 1991). The input to the electron transport model can be an arbitrary electron energy spectrum representing the precipitation at 500 km. The model is parameterised by AP index, F10.7 solar radio flux, the time and geographic location during the period of interest. In this paper, the model has been run for two different PCA events and we have assumed a Gaussian distribution as the input precipitation spectrum for both events. A detailed review of the electron transport model is given in (Lanchester & Gustavsson, 2013).

2.2 Supporting instrumentation

We have also used data from the SSJ/5 particle spectrometers on board DMSP; these instruments provide spectrograms of ion and electron precipitation along the track of the spacecraft and can be used in conjunction with SSUSI to classify different types of polar cap aurora. (Note that references to SSJ/4 in Reidy et al. (2018) should have instead referred to SSJ/5; SSJ/4 is a near identical instrument that was present on previous DMSP satellites). In this paper we have used data from four DMSP spacecraft (F16-F19).

We have used data from the OMNI database (King & Papitashvili, 2005) to provide the IMF conditions during our events. The OMNI database consists of solar wind magnetic field and plasma data sets that have been time-shifted to the nose of the Earth's bow shock and give an estimation of the solar wind conditions at the Earth.

For one event, we have also obtained map potential plots from the SuperDARN radars (Ruohoniemi & Baker, 1998). These data were used to investigate whether the ionospheric flow associated with a polar cap arc is consistent with open field lines, and are presented in section 3.2.

3 Observations

3.1 Closed field line observation

Figure 1 gives a summary of the auroral and IMF conditions for a polar cap arc event which occurred on 4 February 2016. Fig 1a and b demonstrate SSUSI observations from each hemisphere (south and north respectively) with the corresponding DMSP particle data to the right (from DMSP F16 and F17 respectively); these images were chosen to give an overview of the event. The times at the top of the SSUSI images indicate when the DMSP spacecraft was poleward of 70 degrees magnetic latitude (the spacecraft name, orbit number and hemisphere of observation are also given). Estimates of the poleward edge of the auroral oval based on the electron (black) and ion (grey) precipitation measured by the SSJ/5 instruments are indicated in the SSUSI image and SSJ/5 spectrogram; these boundaries were identified using the semi-automated method described in the supplementary material of Reidy et al. (2018). These observations show polar cap arcs occurring on the dawnside of the southern hemisphere and on the duskside of the northern hemisphere that are associated with ion and electron signatures (indicated by

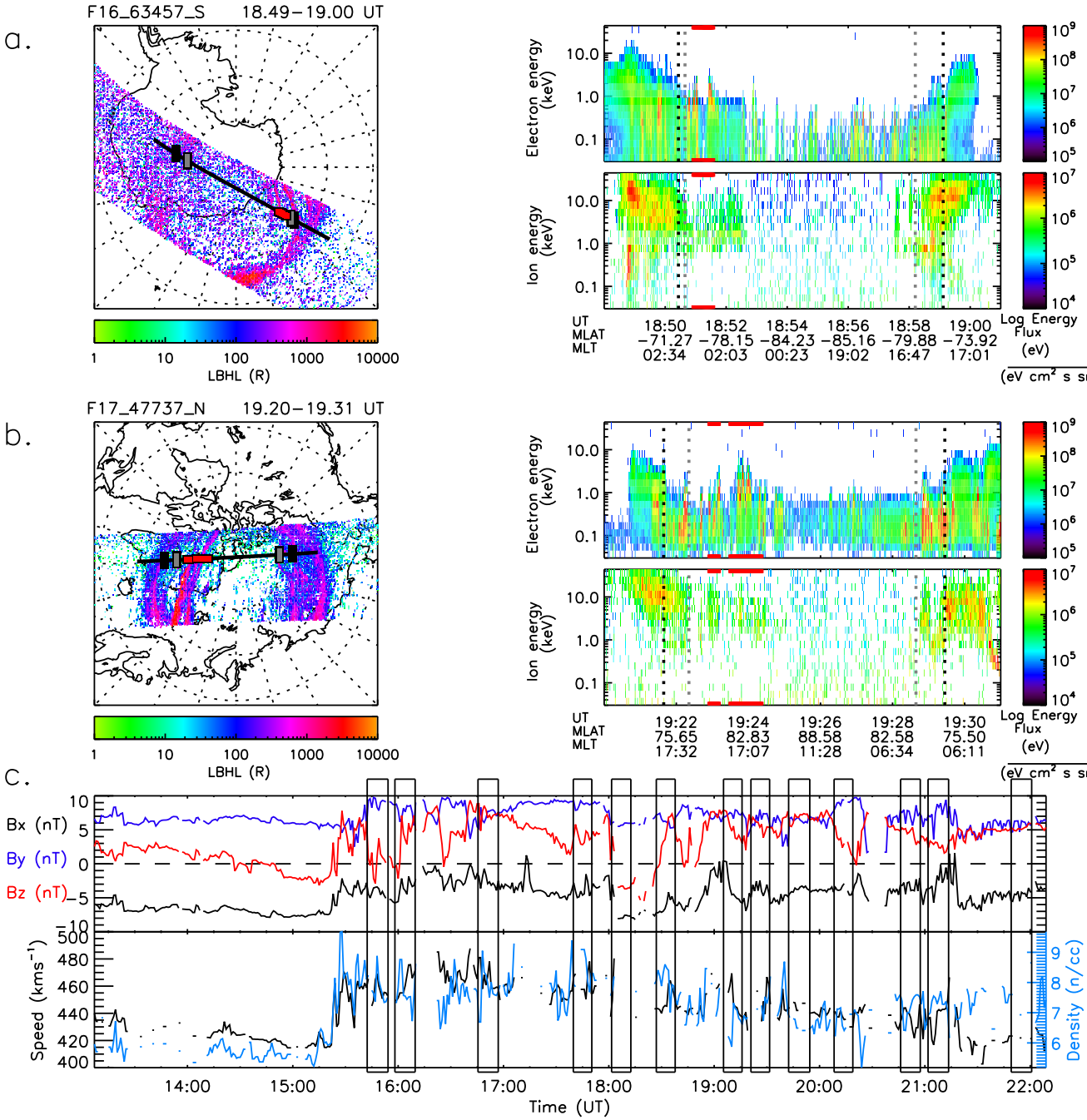

Figure 1. Overview of the 4th February 2016 polar cap arc event. Summary SSUSI and the corresponding SSJ/5 data for the southern hemisphere (a) and the northern hemisphere (b). The top panel of (c) gives the IMF magnetic field B_x, B_y, B_z components in black, blue and red respectively. The bottom panel of (c) gives solar wind speed (black) and density (blue). The times of all the northern hemisphere SSUSI images where a polar cap arc was observed are indicated by boxes.

red lines). According to the criteria and energy flux thresholds described in Reidy et al. (2018), these observations are consistent with polar cap arcs occurring on closed field lines. Furthermore, these arcs occur on opposite sides of the polar cap in each hemisphere consistent with Craven et al. (1991) and Milan et al. (2005). This paper considers only the northern hemisphere SSUSI observations which show polar cap arcs over Svalbard during this event.

Fig 1c shows the magnetic field components (top panel) and the speed and density of the solar wind (bottom panel) during the event. The times of all the northern hemisphere SSUSI images where a polar cap arc was identified during this event are indicated by boxes. The first polar cap arc observations in the northern hemisphere SSUSI images occurred at 15:45 UT. This is shortly after a clear change in the solar wind conditions, at 15:30 UT, where the solar wind speed and density increased and the IMF became strongly northward. During the event the IMF remained predominately northward, with a few short southward turnings, and had negative B_x and positive B_y components. Using the times of the SSUSI images where a polar cap arc was observed, we can assume a minimum event duration of 6 hours, between approximately 16:00-22:00 UT. A maximum event duration of 7 hours can be assumed using the times of the SSUSI observations immediately before and after this interval where a polar cap arc could not be discerned from the UV images. All the northern hemisphere SSUSI observations where a polar cap arc was identified during this event (the times of which correspond to the boxes indicated in Fig. 1c) are given in Figure S1 of the supplementary material.

Figures 2a and b show SSUSI observations, at 18:27-18:37 UT and 19:05-19:15 UT respectively, when the polar cap arc was over Svalbard. Images from the Sony all sky camera have been projected onto the SSUSI images for context. Panels 2c-j show the all-sky images in approximately two minute intervals between 18:40-18:52 UT. The yellow squares in each of the all sky images indicates the approximate field of view of the ASK instrument (which is aligned with magnetic zenith). In these images North is at the top and East is to the left. A bright, approximately north-south aligned arc can be seen passing from East to West (duskward) over magnetic zenith during this interval. The image at 18:48:08 UT (Fig. 2g), is included to show the time when the arc crossed magnetic zenith, which is used for later analysis. This image has been projected onto the SSUSI image in Fig. 2b to show that the two observations are almost perfectly aligned (even though they are occurring at different times). An all sky image prior to this at 18:32:56 UT

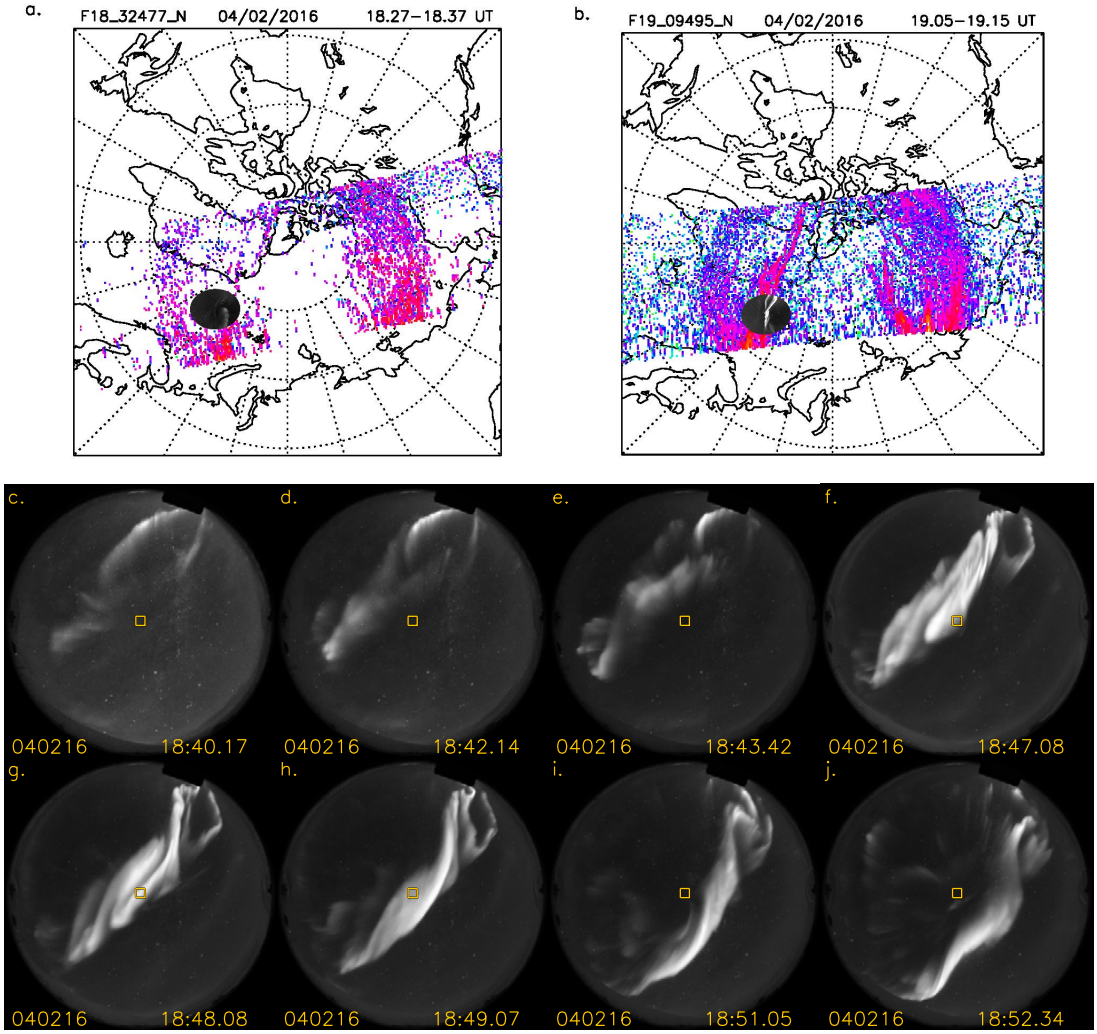

Figure 2. a. A northern hemisphere SSUSI DMSP F18 image between 18:27-18:37 UT. b. A northern hemisphere SSUSI DMSP F19 image between 19:05-19:15 UT. c-j: Images from the Sony all sky camera between 18:40-19:52:30 UT in approximately 2 minute intervals where North is to the top and East is to the left. The yellow box in each image shows the approximate field of view of the ASK instrument. All sky images at 18:32:56 UT and 18:48:08 UT are projected onto the SSUSI images in a and b respectively.

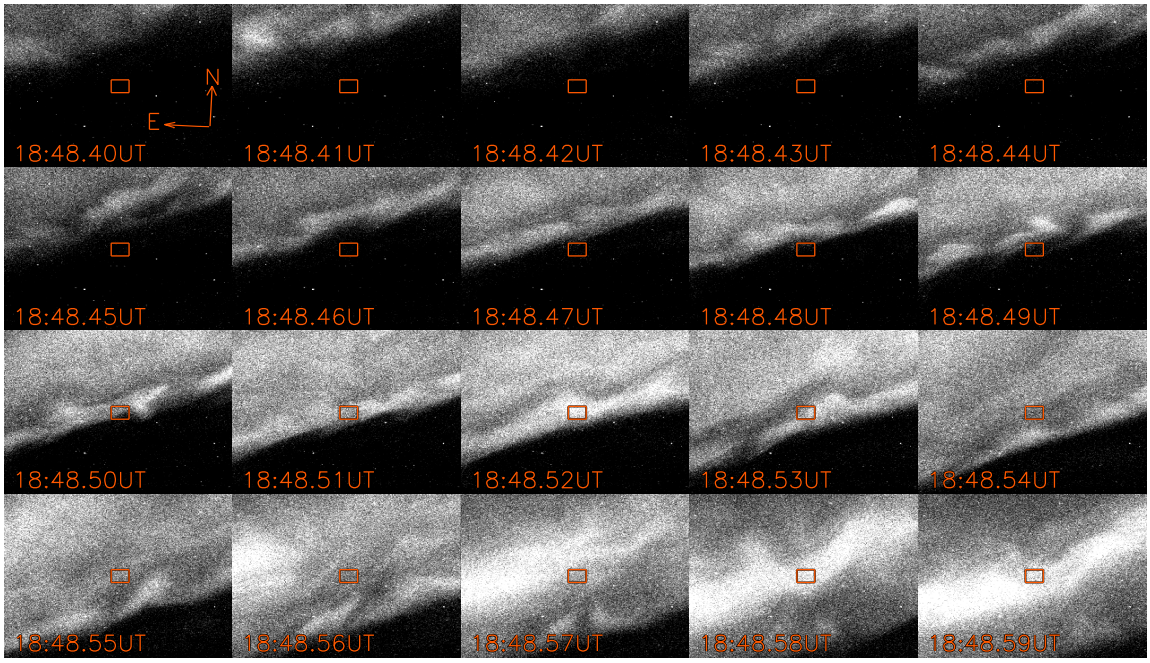

Figure 3. Images from the ASK1 camera at one second resolution between 18:48:40-18:48:59 UT. The red box indicated 20x20 pixels surrounding magnetic zenith. In each image, North is approximately to the top and East to the left.

has also been plotted on the SSUSI image in Fig. 2a to demonstrate that the arc has moved duskward over Svalbard.

Figure 3 shows images from the ASK instrument between 18:48:40-18:48:59 UT, when the arc passed over magnetic zenith. During this event, the ASK instrument was running at 20 frames per second. These images are from the ASK1 camera which has a filter that is sensitive to a prompt emission caused by high energy precipitation. The red boxes in these images indicate the 20 $\times$ 20 pixels surrounding magnetic zenith which are used later for analysis. During this interval an auroral boundary-like form can be seen to sweep across the ASK field of view from a North-East direction, consistent with the direction of the arc seen in the all sky images (Fig. 2). Small scale structures can be seen on the edge of this 'boundary' which are similar to the curls (anti-clockwise vortices with a typical wavelength of 5 km) reported by Vogt et al. (1999), although smaller in size, or are perhaps consistent with the boundary undulations (ruffs) reported by Dahlgren et al. (2010). The highly structured dynamic auroral observations are consistent with previous ASK observations when it was situated in Tromsø under the main auroral oval

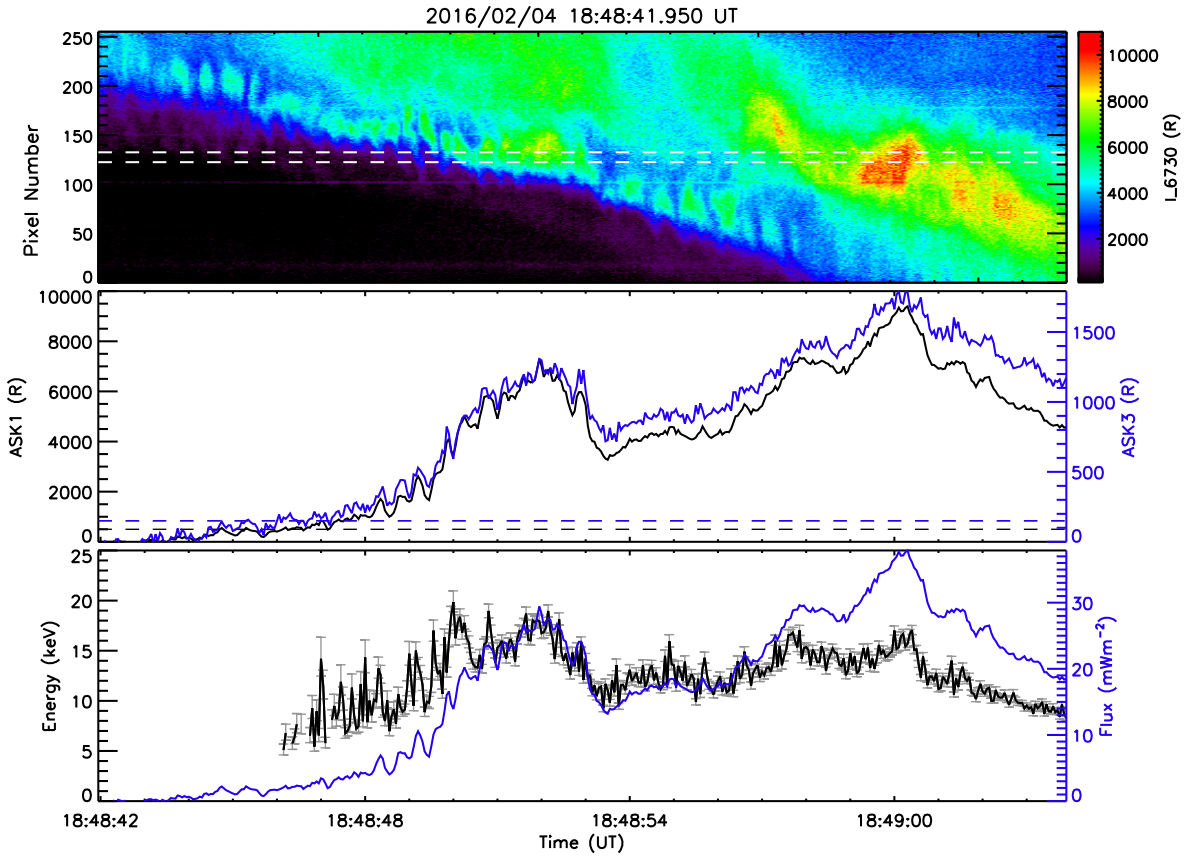

Figure 4. ASK data from a period when the polar cap arc passes through magnetic zenith over Svalbard. The top panel shows a keogram of images from the ASK1 camera. The second panel shows the brightness measured by ASK1 and ASK3 in black and blue respectively; the dashed lines indicate the background level for each channel. The estimated energy (black) and energy flux (blue) are shown in the bottom panel. The error on the energy estimation is shown by grey bars.

(for example, Lanchester et al. (2009); Dahlgren et al. (2010, 2011, 2016)), and are therefore consistent with formation on closed field lines.

Figure 4 shows the ASK observations during our period of interest in a more quantitative way. The top panel shows a keogram of the ASK1 observations between 18:48:42-18:49:04 UT which is made from vertical cuts of the images from ASK1. This keogram clearly shows the repetitive structures on the boundary of the arc discussed above. The second panel of Fig. 4 shows the brightness measured by the ASK1 (black) and ASK3 (blue) cameras in the 20 × 20 pixels around magnetic zenith indicated by the red boxes

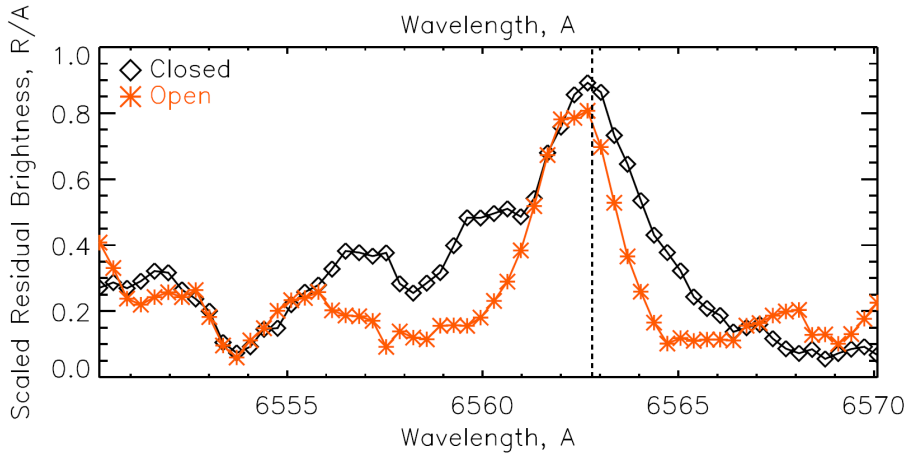

Figure 5. Residual spectra measured by the HITIES instrument between 6550-6570 Å(where 1 Å= 0.1 nm) for the 'closed' (black) and 'open' (red) events.

in Fig. 3 and the white dashed lines in the above keogram. The bottom panel shows the energy (black) and energy flux (blue) estimated by comparing the ratio of the measured brightness from ASK1 and 3 to the Southampton Ionospheric model (as described in Section 2.1.1). We have only calculated the energies when the observed brightness was above a background level which is indicated by horizontal dashed lines in the middle panel. The error on the energy is shown by grey error bars; these errors are propagated from the initial counts measured by the ASK1 and ASK3 cameras. The estimated energies are varying between approximately 5 and 20 keV during this interval, with a mean value of 12.6 $\pm$ 0.9 keV; this value is larger than the mean energy estimated for the 'failed' transpolar arc reported by Reidy et al. (2017), which was found to be 5 keV. Around 18:49:00 UT, a brightening in the keogram (top panel) and a corresponding increase in the brightness (middle panel) can be observed. The bottom panel shows that at this time the energy remained approximately constant but the energy flux increased. These estimates are discussed in Section 4 but for now we note that, due to the high values of the estimated energy and energy flux and the structure of the auroral forms seen in Fig. 3, that these observations are consistent with formation on closed field lines and is referred to as the 'closed' event for the remainder of this paper.

The black line in Figure 5 shows the scaled-residual spectra measured by the H-α panel of the HiTIES instrument, which have been integrated between 18:48:48-18:49:04 UT during this event. The contributions from OH, N_2, N^+ and O_2^+ emissions have been fit-

ted and removed using methods outlined in Chadney and Whiter (2018) and Price et al. (2019), leaving just the H-α emission at 6563 Å(indicated by a vertical dashed line). These observations (as well as the red line) will be discussed in more detail in Sections 3.2 and 4.3 but for now we note the presence of a peak in the black line at 6563 Å which indicates H-α emission, and that the peak appears to be broader towards shorter wavelengths (a 'blue wing', which will be clarified later), consistent with downward accelerated protons.

3.2 Open field line observation

Figure 6 (presented in the same format as Fig. 1) shows the auroral and IMF conditions for a polar cap arc event occurring on 15th December 2015. This event was classified in the Reidy et al. (2018) survey as an event containing multiple arcs consistent with different magnetic field toplogies; polar cap arcs consistent with different magnetic topologies occurring simultaneously were first shown by Reidy et al. (2017). This paper is concerned with the arc on the duskside of the northern hemisphere over Svalbard (shown in Fig. 6a), indicated by orange lines in both the image and the particle data. The corresponding DMSP particle data show that this arc is associated with electron-only precipitation, consistent with accelerated polar rain on open field lines (Newell et al., 2009; Carlson & Cowley, 2005), and thus this event is termed the 'open' event. The arcs on the dawnside associated with ion and electron signatures observed in both hemispheres (indicated by red lines), are not further discussed with respect to the optical observations as they were not observed by the ASK instrument but are considered later with respect to SuperDARN data.

Fig. 6c shows the IMF conditions for this event. Throughout this interval, the IMF was predominately northward with weakly positive B_x and negative B_y components. Similar to Fig. 1, the times of northern hemisphere SSUSI images where the electron-only polar cap arc was identified are indicated by boxes. The times from these SSUSI images can be used to infer a minimum event duration of 35 minutes (between 18:40-19:15 UT), when the arc was observed, and a maximum event duration of 3 hours from the images before and after this time, when the arc was not observed. A more accurate event duration cannot be obtained due to the limited SSUSI observations in the northern hemisphere but we note that this 'open' event is shorter in duration than the 'closed' event presented in Section 3. Observations of this duskside arc from all four SSUSI and SSJ/5

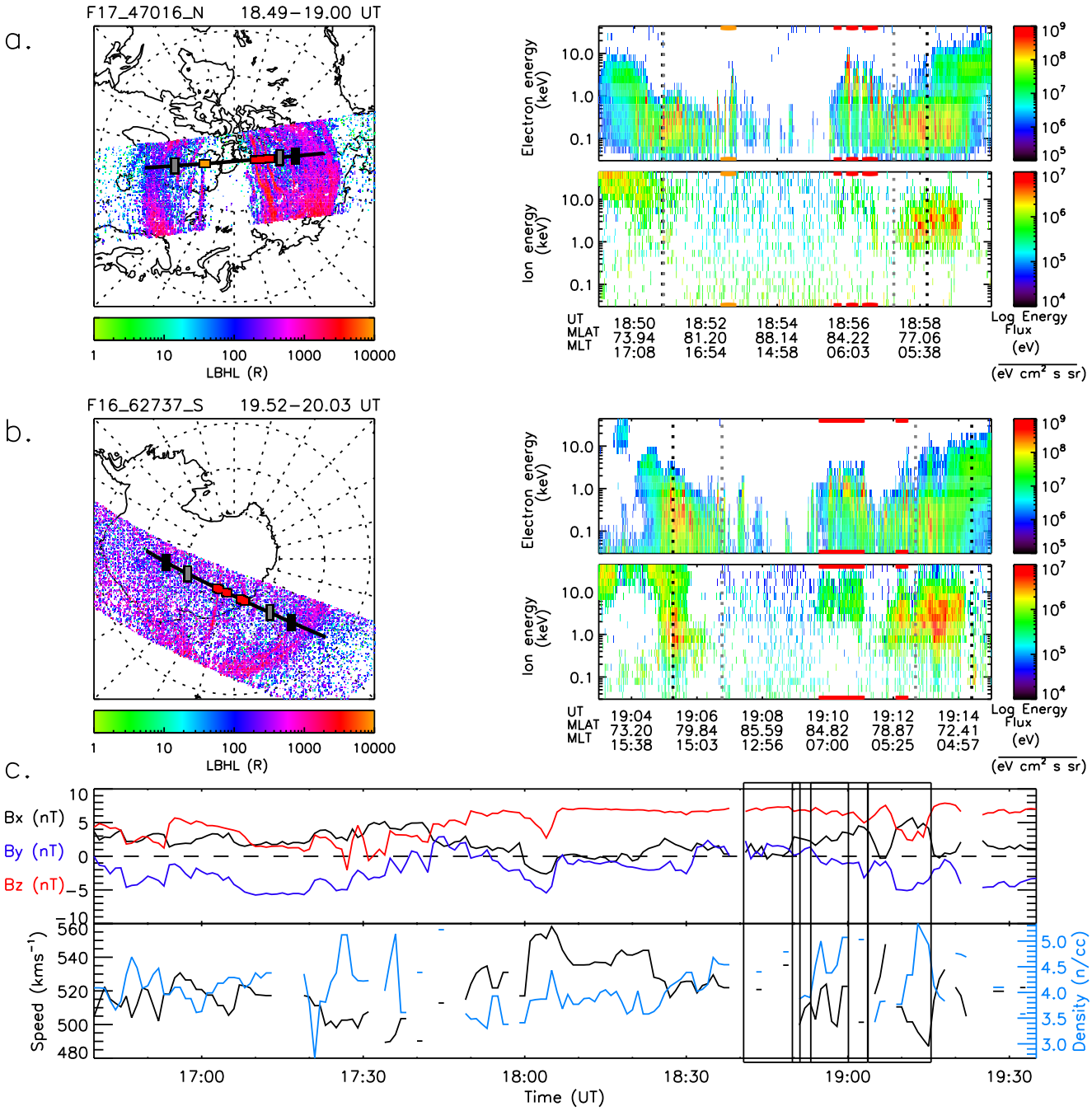

Figure 6. The SSUSI and corresponding SSJ/5 data are shown for the northern hemisphere (a) and southern hemisphere (b) during a polar cap arc event. (c) The magnetic IMF components of the IMF are given in the top panel, the solar wind speed and density in the bottom panel. Times of the SSUSI observations are indicated by boxes.

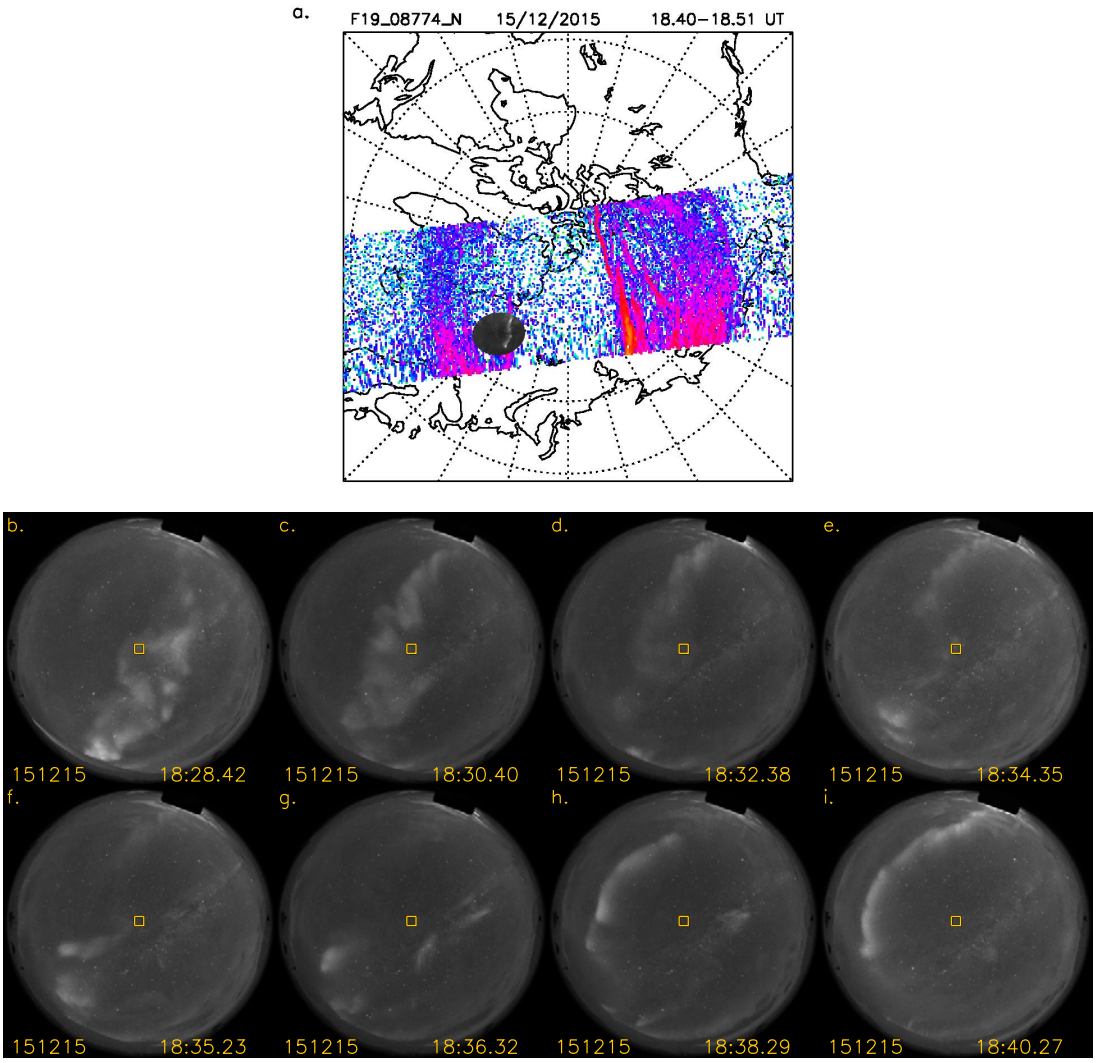

Figure 7. a. A SSUSI image from DMSP F19 between 18:40-18:51 UT with an all sky image at 18:41 UT projected onto the same MLT grid. b-i: images from the Sony all sky camera between 18:28-18:40UT, with North to the top and East to the right.

instruments on board the different DMSP spacecraft are given in Figure S2 of the supplementary material. The electron-only signature associated with the arc is observed by all four SSJ/5 instruments.

The SSUSI DMSP F19 observations between 18:40-18:51 UT are replotted in Figure 7a, with images from the Sony all sky camera in 2 minute intervals between around 18:28-18:40 UT (Figs. 7b-i). This is the interval in which a roughly north-south aligned arc passed through the ASK field of view, indicated by yellow boxes on each of the all

sky images (same as Fig. 2). Fig. 7f shows the time when an arc was seen by ASK, around 18:35 UT. From the all-sky images it appears that a feature passes over the ASK field of view between Figs. 7b and c, however, no clear structure could be distinguished in the ASK instrument at this time as this feature was too diffuse to be identified in the small field of view of ASK. An all sky image at 18:41:06 UT has been projected onto the SSUSI DMSP F19 image in Fig. 7a as this image was closest to the time when the polar cap arc was observed by the SSUSI instrument. This projection demonstrates that the approximately north-south arc passing through the field of view of ASK is aligned with the polar cap arc seen in the SSUSI images.

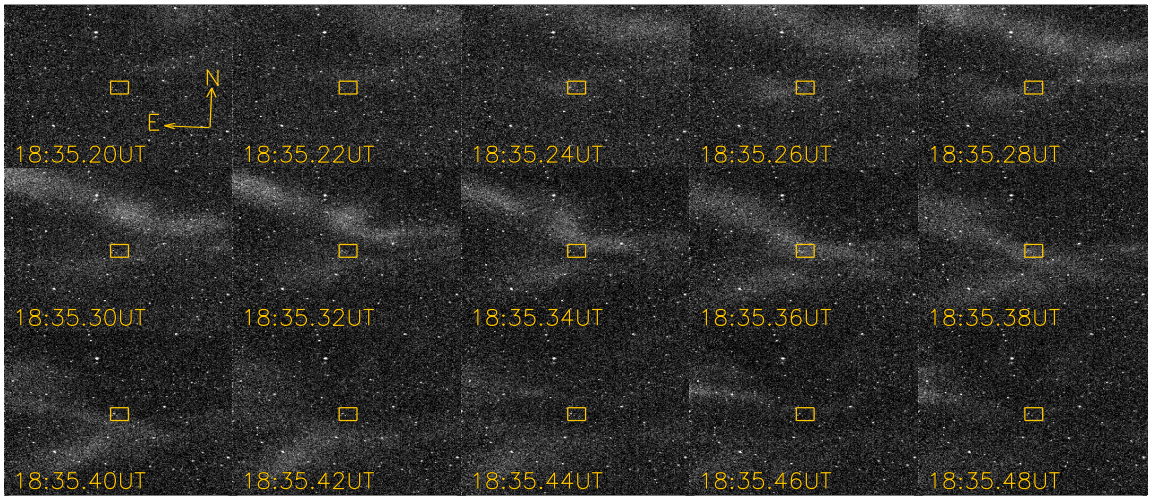

Figure 8. Stills from the ASK3 camera between 18:35.20-18:35:48 UT when the 'open' field line arc passed through magnetic zenith.

Figure 8 shows stills from the ASK 3 camera between 18:35:20-18:35:48 UT, which correspond most closely to Fig. 7f. The ASK3 filter is more sensitive to lower energy precipitation and in this event shows the auroral observations more clearly than the ASK1 camera (as opposed to the closed event which was clearest in the high-energy sensitive ASK1 filter). Due to these observations being very faint, it was necessary to average the images produced at 20 frames per second over two minutes to discern any structure in this event. As well as being much fainter than the 'closed' event, the structure of the 'open' arc is much less continuous in the times between the image frames. Here the arc is not as north-south aligned as it appears in the all sky images however ASK is observing only a small part of the overall arc which has a wave-like appearance as in evident in Fig. 7c.

Some faint structure is visible on the northward edge of the arc in the ASK field of view passing from the north-west direction (around 18:35:32 UT) but is very hard to distinguish. It is possible that some of the auroral structure has been lost due to the averaging, which is comparable to the timescales of the structure seen in the closed event (i.e. less that 2 seconds). Although a more detailed description of this 'open' structure cannot be given due to the weakness of the emission, it is clearly very different from the dynamic 'closed' event presented in Section 2.

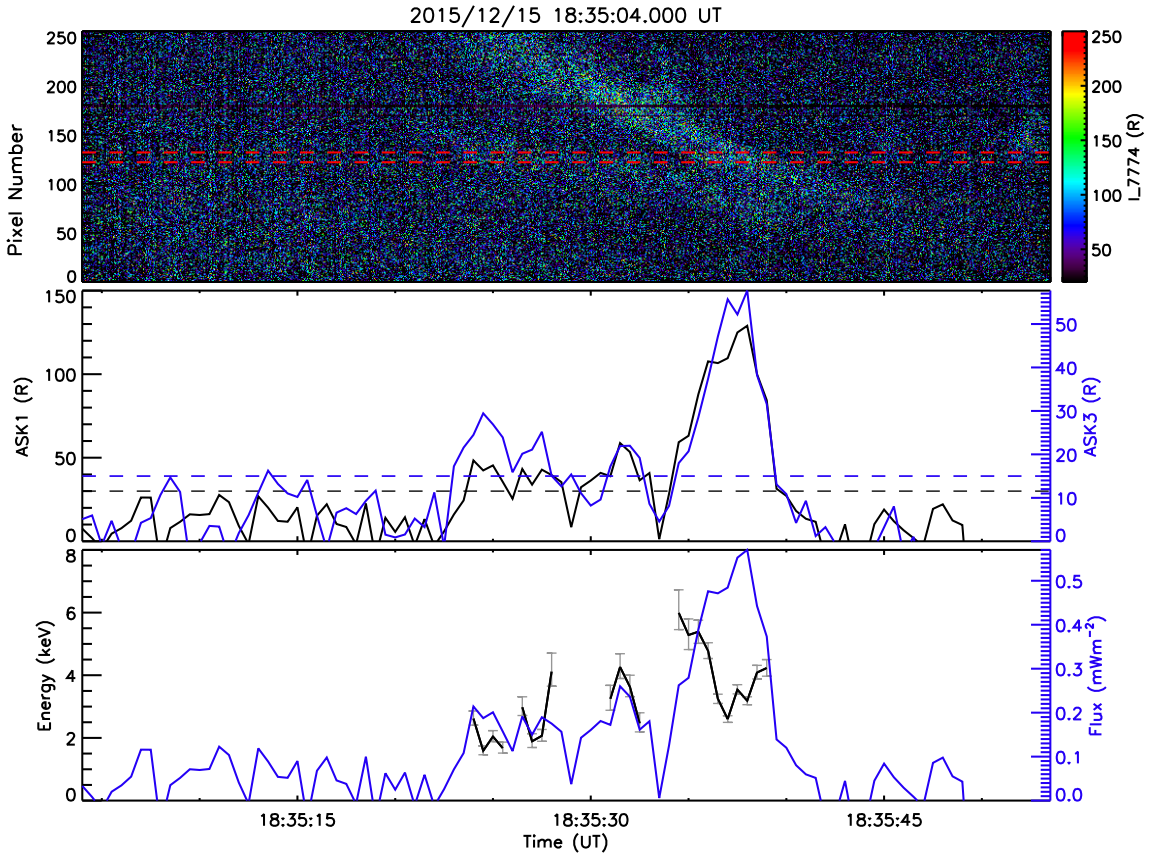

Figure 9. ASK data from a period when the polar cap arc consistent with open field lines passes through magnetic zenith over Svalbard. In the same format as Fig. 4

Figure. 9 (similar to Fig. 4) shows the ASK data in keogram format, along with the brightness at magnetic zenith and the energies and energy flux estimates. The pixels averaged over magnetic zenith are shown by red dashed lines on the keogram. As for the 'closed' case, the energies are only estimated above a background level which is indicated by dashed lines in panel 2. However, as the brightness of the emissions are sig-

nificantly lower in this case, the brightness is above the background for a shorter portion of the event. The arc can be seen to pass through magnetic zenith around 18:35.35 UT with a mean energy of approximately 3.4 ± 0.1 keV. As is evident from the ASK 3 stills in Fig. 8 and from panel 2 of Fig. 9, this event is of much lower brightness than the 'closed' event (Fig. 4). The lower flux and brightness associated with this 'open' arc are consistent with the low plasma density of the magnetotail lobes.

The red line in Figure 5 shows the scaled-residual spectra measured by the H-α panel of the HiTIES instrument during the 'open' event, integrated between 18:35:00 UT and 18:36:10 UT. As before, a fit for the spectra (excluding H-α) has been obtained using methods outlined in Chadney and Whiter (2018) and Price et al. (2019) which has then been taken away from the integrated spectra. Similarly to the 'closed' event, H-α emission is present, at 6563 Å, but here the emission is much narrower in its wavelength extent. These observations will be discussed further in Section 4.3.

Figure 10 shows a series of SuperDARN map potential plots between 18:36-18:42 UT overlaid on the SSUSI DMSP F19 image between 18:40-18:51 UT (shown in Fig. 7a.). Evidence of lobe reconnection can be seen in all of the images with the merging gap (the footprint of the reconnection site, identified by a region of sunward flow) slightly dawnward of noon, around 80° magnetic latitude. On the dawnside of the polar cap, ionospheric scatter can be seen near the (closed field line) dawnside arc, with anti-sunward flow seen between the arc and the oval. Duskward of the 'closed' dawnside arc not yet discussed in this paper, scatter is only observed at the sunward tip of the arc, but here we see the flows are sunward and therefore the arc is aligned with the sunward flow channel into the merging gap. The clockwise motion of this dawnside lobe convection cell is consistent with upward field aligned current and hence downward electron precipitation (e.g. Chiu et al. (1985)). However, in the Chiu et al. (1985) model, they predict the arc to be located in the center of the flow cell whereas around 18:40 UT (Fig. 10c), at the time of the SSUSI image, observations show the tip of the arc to be aligned with the sunward flow. This is inconsistent with the Chiu et al. (1985) prediction but is consistent with Fear et al. (2015), who argued that a polar cap arc should be drawn towards the sunward flow channel by the flows themselves.

On the duskside, there is not much scatter around the 'open' polar cap arc of interest to this study, particularly on the nightside. In Figs 10a and b, the lobe convec-

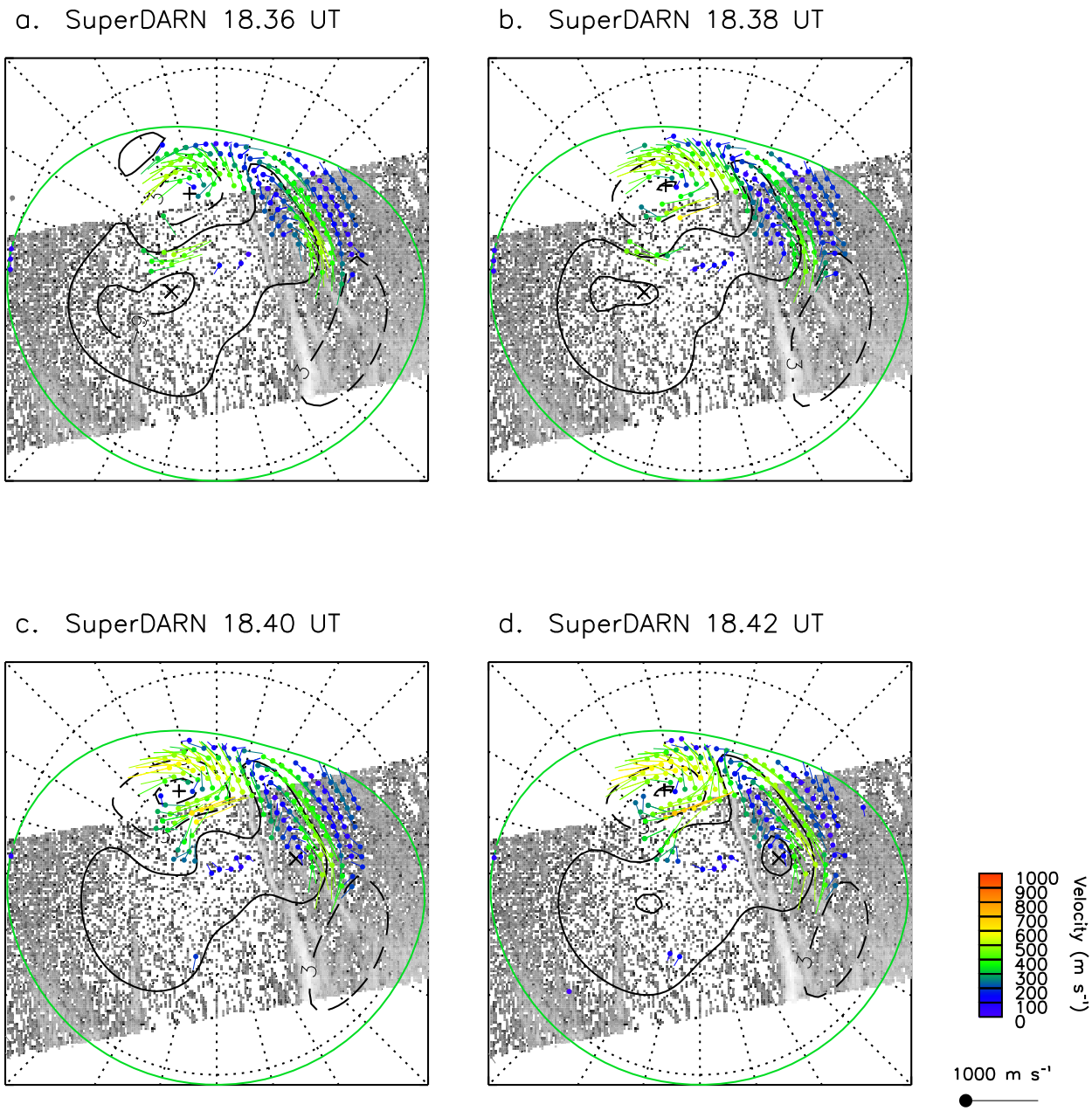

Figure 10. SuperDARN map potential plots between 18:36-18:42 UT over plotted on a SSUSI DMSP F19 image between 18:40-18:51 UT. The ionospheric flow measurements are indicated by a circle with a line attached (shown in the bottom right corner), the colour of which gives the magnitude of flow and the line shows the direction. The contours show a model fit of the flows constrained by the data and IMF conditions, the × and + are the minimum/maximum of this potential distribution, where the negative potential contours are shown by solid lines and positive contours are dashed. The green circle is the Heppnar Maynard Boundary.

tion cell appears to be sunward of the 'open' arc. In Figs. 10c and d, the sunward tip of the arc is approximately aligned with the duskward edge of the sunward flow channel. This alignment could be consistent with Fear et al. (2015) but is again inconsistent with a direct application of the arguments of Chiu et al. (1985) as the arc is not centred on what we can see of the dusk convection cell; even if it were, the sense of the rotation of the flow would suggest a downward current and hence upward-moving electrons. In the absence of more extensive scatter coincident with the duskside open arc, we cannot comment conclusively on the cause of this arc. However, we speculate from our knowledge of the sunward extent of the flow pattern that if the duskside arc is caused by a shear flow (as suggested by (Carlson & Cowley, 2005), then this shear is more likely to arise from a gradient in the strength of the sunward flow excited by lobe reconnection, rather than by the opposite flows on either side of the convection cell as envisaged by Chiu et al. (1985).

4 Discussion

4.1 Comparison of small-scale optical observations

The ASK observations for the 'closed' event (Figs. 3 and 4) were seen to be much brighter than for the 'open' event (Figs. 8 and 9). The brightness observed in ASK1 and hence the estimated flux (which depends on this parameter) were approximately 60 times greater for the 'closed' event than for the 'open' event. These lower fluxes for the 'open' event are consistent with a topological connection to the open field lines of the magnetotail lobes, where the plasma population is low. The energies of the two events are more comparable, with mean values of 12.6 $\pm$ 0.9 keV estimated for the 'closed' case and 3.4 $\pm$ 0.1 keV estimated for the 'open' case. Carlson and Cowley (2005) state that any mechanism which drives shear flow across open field lines can accelerate polar rain and generate aurora on open field lines in the polar cap. They also estimate, for three sub-visual polar cap arcs (which refer to arcs lower than 1 kR and are consistent with our 'open' observation), energies between 100-1000 eV which they state are consistent with Shinohara and Kokubun (1996) and Hardy (1984). Therefore our mean value for the energy of the 'open' event from the ASK analysis is larger than previous reports. This will be further discussed below when we compare the ASK analysis to the DMSP particle data observations.

The structure of the arcs as they pass through ASK's 6° field of view are quite different in appearance; the aurora in the 'closed' event (Fig. 3) was highly dynamic and structured (especially on the edges of the arc), similar to structure observed within the main auroral oval (e.g. Dahlgren et al. (2010)). In the open case the aurora appeared unstructured; however, the averaging of images because of the low fluxes may have blurred any existing faint structures.

4.2 Comparison of ground-based and spacecraft measurements

4.2.1 Energy flux measurements

Figures 11a and b show one minute of data from the SSJ/5 instrument when the DMSP spacecraft intersected the polar cap arcs for the 'closed' and 'open' events respectively; the top panel gives the integrated energy flux and the bottom panel shows the electron spectrogram. The mean energy flux and the mean energy estimated from the ASK instrument (Figs. 4 and 9) are shown by red lines. It can be seen in the top panel of Fig. 11a, for the 'closed' event, that the mean energy flux estimated by ASK (20.1 mW m^{-2}) agrees well with the energy flux recorded by the DMSP spacecraft, despite the two values being determined at different times and locations in the polar cap (DMSP F19 in-situ measurements are from 19:24 UT and the ASK measurements are from approximately 18:49 UT, also the DMSP spacecraft are orbiting closer to the dayside than Svalbard during this interval). In the top panel of Fig. 11b, for the 'open' event, it can be see than the energy flux measured by the DMSP spacecraft is approximately a factor of 10 greater than the mean energy flux estimated from the ASK analysis (0.3 mW m^{-2}). As discussed above these measurements are at different times (DMSP observations are at 18:53:30 UT whereas the ASK observations are from 18:35:30 UT) and therefore some discrepancies are expected. However, the difference in energy flux can also be understood in terms of the spatial separation between the two observation points. The DMSP pass occurs on the dayside of the polar cap whereas Svalbard is located on the nightside during this interval; therefore a physical reason for the discrepancy in the observations could be due to the noon-midnight gradient in the polar rain flux. This was first explicitly shown by Newell et al. (2009) and is due to the the kink in the open field lines as they cross the polar cap and enter the magnetotail. For particles to enter the ionosphere via these open field lines they have to have thermal speeds greater than the bulk plasma velocity, which is approximately the kink speed of the magnetic field lines. Fewer particles are able to

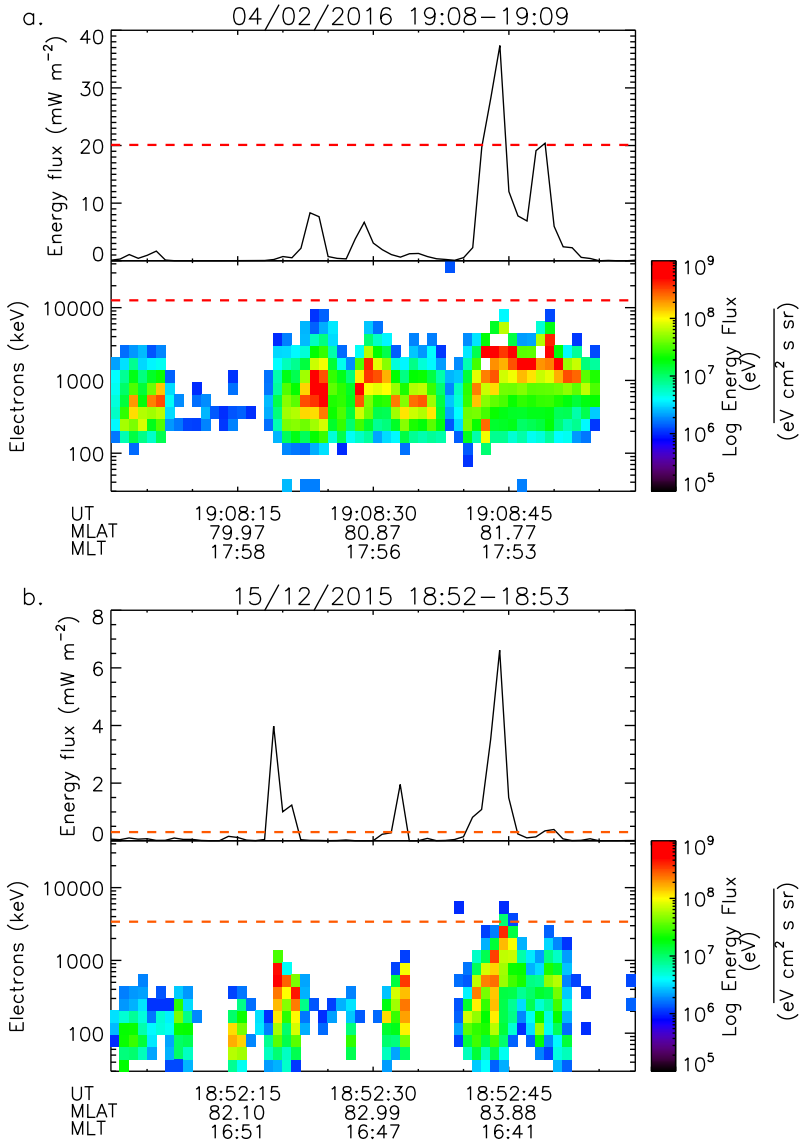

Figure 11. The summed energy flux (top panel) and corresponding electron spectrograms (bottom panel) for the 'closed' (a) and 'open' (b) events over one minute as the DMSP F19 and F17 spacecraft intersected the arcs respectively. The red lines show the approximate energy flux and energy estimated using ground based techniques.

enter the ionosphere as the field lines travel further downtail, which leads to a drop off in the polar rain flux across the polar cap. This gradient is consistent with our observations and could therefore explain the discrepancies between the DMSP and ASK observations for the 'open' event.

4.2.2 Energy measurements

The energies plotted in the bottom panels of Figs. 4 and 9 represent the characteristic energy of the precipitation from a Gaussian distribution. The SSJ/5 spectrograms in Figure 11 show the energy distributed over a log scale. It can be seen that the estimated energy for the 'open field line' event (Fig. 11b), despite being larger than previous estimates for polar rain arcs as discussed above, agrees well with the DMSP particle data. In the case of the 'closed field line' event (Fig. 11a) the energy estimate from the ground-based techniques is slightly larger than measurements from DMSP. Considering the polar cap arc formation mechanism suggested by Milan et al. (2005) (which describes nightside reconnection during northward IMF where the newly closed field lines get 'stuck' in the magnetotail), this potential discrepancy can be understood in terms of field line contraction. The DMSP observations are further sunward when considering the ionospheric footprint of the field line than those over the ASK instrument (see Fig. 1), this means that the closed field line associated with the DMSP observation crosses the equator further tailward. The field line over the ASK instrument will be closer to the planet at the equator and therefore more contracted than the field lines sampled by the DMSP spacecraft. Therefore, we may expect the electrons causing the ASK precipitation to have undergone more acceleration (and therefore be at higher energies) than electrons on field lines further sunwards, like those over DMSP, consistent with our observations.

4.3 Ground-based spectral observations

As previously discussed, Fig. 5 shows the residual fit from the H-α panel of the HiTIES instrument, between 6550-6570 Å, for the 'closed' and 'open' events in black and red respectively. During the 'closed' event, there is an additional broadening towards shorter wavelength which indicates a Doppler shifted blue wing generated by precipitating protons (e.g. Eather (1967)). In the 'open' case, the spectrum is centred on the unshifted H-alpha wavelength, with no raised wings, which suggests that the emission is a result

of dayglow (Weller et al., 1971). These observations are consistent with the DMSP observations and demonstrate that the auroral precipitation used to identify the topology of the field lines on which the polar cap arcs are formed, can be verified using ground-based instrumentation.

4.4 Ionospheric flow observations

SuperDARN map potential plots were shown in context with SSUSI observations during the 'open' event (Fig. 10); evidence of lobe reconnection was seen throughout the event. These data were initially investigated to try to find evidence of shear flows which could be accelerating polar rain and generating this arc (as suggested by Carlson and Cowley (2005)). However, the ionospheric flows associated with the lobe reconnection cell on the duskside were anti-clockwise which is not consistent with upward field aligned current or precipitating electrons (Chiu et al., 1985). Furthermore, we note that scatter confirming the presence of this convection cell was only present sunward of the 'open' arc, and we therefore have insufficient information on the presence or absence of shear flows at the location of the arc. We speculate that, if a shear flow does exist, rather than it being generated by opposing flow shears, as envisaged by (Chiu et al., 1985), it is more likely to be excited by the gradient in the strength of the sunward flow generated by the lobe reconnection, due to the location of the sunward flow. We also noted that the sunward tips of both of the arcs observed in this event (the 'open' arc on the duskside discussed in this paper and the arc consistent with closed field lines on the dawnside), were aligned with the sunward flow channels generated with lobe reconnection, in agreement with Fear et al. (2015), as opposed to being centered between the opposing flow channels suggested by Chiu et al. (1985).

5 Conclusion

Two events containing polar cap arcs occurring over Svalbard on 15/12/15 and 04/02/16 have been investigated using multi-scale ground based and spacecraft instrumentation. The arcs were classified as consistent with occurrence on different magnetic topologies in each event, based on the associated particle precipitation and if there were observed in SSUSI images from one or both hemispheres (as discussed in Reidy et al. (2018)). The arcs were analysed using ground based instrumentation on Svalbard including an all sky imager, a high resolution multi-spectral imager (ASK) and a spectrograph (HITIES).

The all sky images showed approximately North-South aligned arcs passing through the field of view of ASK that mapped to the locations of the polar cap arcs observed in SSUSI UV images.

Key findings:

- This paper expands the knowledge of polar cap arcs by presenting the first observations of polar cap arcs on very small spatial scales (of the order of meters) and temporal resolution (milliseconds to seconds) using the ASK instrument.
- The structure associated with arcs generated by different formation mechanisms is found to be very different and fits with expectations for the different magnetic field topologies, i.e. polar cap arcs on closed field lines were found to be associated with dynamic structured aurora whereas arcs formed on open field lines were found to be associated with much lower fluxes and less structure.
- Estimates of the energy and energy flux of the precipitation generating these arcs from the ASK observations were compared with in-situ measurements from the DMSP spacecraft. We found generally good agreement between the two and were able to explain any potential inconsistencies by considering the location where the measurement were taken with respect to each other and to the geometry of the magnetic field lines, and also by considering the nature of the different polar cap arc generation mechanisms.
- During the event containing arcs consistent with closed field lines, a signature of proton precipitation was observed in ground-based data which was not present in the data during the 'open' event. This verifies the criteria outlined by Reidy et al. (2018), for identifying polar cap arcs occurring on different magnetic field topologies by the associated particle precipitation, using independent measurements from the HiTIES instrument.
- The formation mechanisms of polar cap arcs occurring on open field line arcs have been investigated using measurements of the ionospheric flows associated with lobe reconnection using SuperDARN. A gradient in these flows is suggested to be a possible source of the shear flow which could result in downward current and acceleration of polar rain.

References

Berkey, F. T., Cogger, L. L., Ismail, S., & Kamide, Y. (1976). Evidence for a correlation between sun-aligned arcs and the interplanetary magnetic field direction. *Geophysical Research Letters*, *3*, 145-147. doi: 10.1029/GL003i003p00145

Carlson, H. C., & Cowley, S. W. H. (2005). Accelerated polar rain electrons as the source of Sun-aligned arcs in the polar cap during northward interplanetary magnetic field conditions. *Journal of Geophysical Research*, *110*, A05302. doi: 10.1029/2004JA010669

Carter, J. A., Milan, S. E., Fear, R. C., Walach, M.-T., Harrison, Z. A., Paxton, L. J., & Hubert, B. (2017). Transpolar arcs observed simultaneously in both hemispheres. *Journal of Geophysical Research*, *122*(6), 6107–6120. (2016JA023830) doi: 10.1002/2016JA023830

Chadney, J. M., & Whiter, D. K. (2018). Neutral temperature and atmospheric water vapour retrieval from spectral fitting of auroral and airglow emissions. *Geoscientific Instrumentation, Methods and Data Systems*, *7*(4), 317–329. doi: 10.5194/gi-7-317-2018

Chakrabarti, S., Pallamraju, D., Baumgardner, J., & Vaillancourt, J. (2001). HiTIES: A high throughput imaging echelle spectrograph for ground-based visible airglow and auroral studies. *Journal of Geophysical Research*, *106*, 30337-30348. doi: 10.1029/2001JA001105

Chiu, Y. T., Crooker, N. U., & Gorney, D. J. (1985). Model of oval and polar cap arc configurations. *Journal of Geophysical Research*, *90*, 5153-5157. doi: 10.1029/JA090iA06p05153

Craven, J. D., Murphree, J. S., Cogger, L. L., & Frank, L. A. (1991). Simultaneous optical observations of transpolar arcs in the two polar caps. *Geophysical Research Letters*, *18*, 2297-2300. doi: 10.1029/91GL02308

Dahlgren, H., Aikio, A., Kaila, K., Ivchenko, N., Lanchester, B. S., Whiter, D. K., & Marklund, G. T. (2010). Simultaneous observations of small multi-scale structures in an auroral arc. *Journal of Atmospheric and Solar-Terrestrial Physics*, *72*, 633-637. doi: 10.1016/j.jastp.2010.01.014

Dahlgren, H., Gustavsson, B., Lanchester, B. S., Ivchenko, N., Brändström, U., Whiter, D. K., ... Marklund, G. (2011). Energy and flux variations across thin auroral arcs. *Annales Geophysicae*, *29*, 1699-1712. doi:

10.5194/angeo-29-1699-2011

Dahlgren, H., Ivchenko, N., Sullivan, J., Lanchester, B. S., Marklund, G., & Whiter, D. (2008). Morphology and dynamics of aurora at fine scale: first results from the ASK instrument. *Annales Geophysicae*, *26*, 1041-1048. doi: 10.5194/angeo-26-1041-2008

Dahlgren, H., Lanchester, B. S., Ivchenko, N., & Whiter, D. K. (2016). Electrodynamics and energy characteristics of aurora at high resolution by optical methods. *Journal of Geophysical Research*, *121*, 5966-5974. doi: 10.1002/2016JA022446

Eather, R. H. (1967). Auroral proton precipitation and hydrogen emissions. *Reviews of Geophysics*, *5*(3), 207–285. doi: 10.1029/RG005i003p00207

Fear, R. C. (2019). The northward IMF magnetosphere in Magnetospheres in the Solar System. In H. H. R. Maggiolo N. André & D. Welling (Eds.), *Agu centennial monograph.* Wiley, in press.

Fear, R. C., & Milan, S. E. (2012a). The IMF dependence of the local time of transpolar arcs: Implications for formation mechanism. *Journal of Geophysical Research*, *117*, A03213. doi: 10.1029/2011JA017209

Fear, R. C., & Milan, S. E. (2012b). Ionospheric flows relating to transpolar arc formation. *Journal of Geophysical Research*, *117*, A09230. doi: 10.1029/2012JA017830

Fear, R. C., Milan, S. E., Carter, J. A., & Maggiolo, R. (2015). The interaction between transpolar arcs and cusp spots. *Geophysical Research Letters*, *42*, 9685-9693. doi: 10.1002/2015GL066194

Fear, R. C., Milan, S. E., Maggiolo, R., Fazakerley, A. N., Dandouras, I., & Mende, S. B. (2014). Direct observation of closed magnetic flux trapped in the high-latitude magnetosphere. *Science*, *346*, 1506-1510. doi: 10.1126/science.1257377

Frank, L. A., Craven, J. D., Burch, J. L., & Winningham, J. D. (1982). Polar views of the Earth's aurora with Dynamics Explorer. *Geophysical Research Letters*, *9*, 1001-1004. doi: 10.1029/GL009i009p01001

Goudarzi, A., Lester, M., Milan, S. E., & Frey, H. U. (2008). Multi-instrumentation observations of a transpolar arc in the northern hemisphere. *Annales Geophysicae*, *26*, 201-210. doi: 10.5194/angeo-26-201-2008

Gussenhoven, M. S., Hardy, D. A., Heinemann, N., & Burkhardt, R. K. (1984). Morphology of the polar rain. *Journal of Geophysical Research*, *89*, 9785-9800. doi: 10.1029/JA089iA11p09785

Hardy, D. A. (1984). Intense fluxes of low energy electrons at geomagnetic latitudes above 85°. *Journal of Geophysical Research*, *89*, 3883-3892. doi: 10.1029/JA089iA06p03883

Hardy, D. A., Burke, W. J., & Gussenhoven, M. S. (1982). DMSP optical and electron measurements in the vicinity of polar cap arcs. *Journal of Geophysical Research*, *87*, 2413-2430. doi: 10.1029/JA087iA04p02413

Hedin, A. E. (1991). Extension of the MSIS thermosphere model into the middle and lower atmosphere. *Journal of Geophysical Research*, *96*, 1159-1172. doi: 10.1029/90JA02125

King, J. H., & Papitashvili, N. E. (2005). Solar wind spatial scales in and comparisons of hourly Wind and ACE plasma and magnetic field data. *Journal of Geophysical Research*, *110*, A02104. doi: 10.1029/2004JA010649

Lanchester, B., & Gustavsson, B. (2013). Imaging of aurora to estimate the energy and flux of electron precipitation. In *Auroral phenomenology and magnetospheric processes: Earth and other planets* (p. 171-182). American Geophysical Union (AGU). Retrieved from `https://agupubs.onlinelibrary.wiley.com/doi/abs/10.1029/2011GM001161` doi: 10.1029/2011GM001161

Lanchester, B. S., Ashrafi, M., & Ivchenko, N. (2009). Simultaneous imaging of aurora on small scale in OI (777.4 nm) and $N_2$1P to estimate energy and flux of precipitation. *Annales Geophysicae*, *27*, 2881-2891. doi: 10.5194/angeo-27-2881-2009

Lummerzheim, D., & Lilensten, J. (1994). Electron transport and energy degradation in the ionosphere: evaluation of the numerical solution comparison with laboratory experiments and auroral observations. *Ann. Geophys.*, *12*, 1039-1051.

Meng, C.-I. (1981). Polar cap arcs and the plasma sheet. *Geophysical Research Letters*, *8*, 273-276. doi: 10.1029/GL008i003p00273

Milan, S. E., Hubert, B., & Grocott, A. (2005). Formation and motion of a transpolar arc in response to dayside and nightside reconnection. *Journal of Geophysical Research*, *110*, A01212. doi: 10.1029/2004JA010835

Newell, P. T., Liou, K., & Wilson, G. R. (2009). Polar cap particle precipitation and aurora: Review and commentary. *Journal of Atmospheric and Solar-Terrestrial Physics*, *71*, 199-215. doi: 10.1016/j.jastp.2008.11.004

Paxton, L. J., Morrison, D., Zhang, Y., Kil, H., Wolven, B., Ogorzalek, B. S., ... Meng, C.-I. (2002). Validation of remote sensing products produced by the Special Sensor Ultraviolet Scanning Imager (SSUSI): a far UV-imaging spectrograph on DMSP F-16. In A. M. Larar & M. G. Mlynczak (Eds.), *Optical spectroscopic techniques, remote sensing, and instrumentation for atmospheric and space research iv* (Vol. 4485, p. 338-348). doi: 10.1117/12.454268

Price, D. J., Whiter, D. K., Chadney, J. M., & Lanchester, B. S. (2019). High resolution optical observations of neutral heating associated with the electrodynamics of an auroral arc. *JGR (accepted)*. doi: 10.1029/2019JA027345

Reidy, J. A., Fear, R. C., Whiter, D. K., Lanchester, B., Kavanagh, A. J., Milan, S. E., ... Zhang, Y. (2018). Interhemispheric survey of polar cap aurora. *Journal of Geophysical Research: Space Physics*, *123*(9), 7283-7306. doi: 10.1029/2017JA025153

Reidy, J. A., Fear, R. C., Whiter, D. K., Lanchester, B. S., Kavanagh, A. J., Paxton, L. J., ... Lester, M. (2017). Multi-instrument observation of simultaneous polar cap auroras on open and closed magnetic field lines. *Journal of Geophysical Research (Space Physics)*, *122*, 4367-4386. doi: 10.1002/2016JA023718

Ruohoniemi, J. M., & Baker, K. B. (1998). Large-scale imaging of high-latitude convection with Super Dual Auroral Radar Network HF radar observations. *Journal of Geophysical Research*, *103*, 20797-20811. doi: 10.1029/98JA01288

Shinohara, I., & Kokubun, S. (1996). Statistical properties of particle precipitation in the polar cap during intervals of northward interplanetary magnetic field. *Journal of Geophysical Research*, *101*, 69-82. doi: 10.1029/95JA01848

Vogt, J., Frey, H. U., Haerendel, G., Höfner, H., & Semeter, J. L. (1999). Shear velocity profiles associated with auroral curls. *Journal of Geophysical Research*, *104*, 17277-17288. doi: 10.1029/1999JA900148

Weller, C. S., Meier, R. R., & Tinsley, B. A. (1971). Simultaneous measurements of the hydrogen airglow emissions of Lyman alpha, Lyman beta, and Balmer alpha. *Journal of Geophysical Research*, *76*, 7734. doi: 10.1029/JA076i031p07734

Whiter, D. K., Lanchester, B. S., Gustavsson, B., Ivchenko, N., & Dahlgren, H. (2010). Using multispectral optical observations to identify the acceleration mechanism responsible for flickering aurora. *Journal of Geophysical Research*, *115*, A12315. doi: 10.1029/2010JA015805

Xing, Z., Zhang, Q., Han, D., Zhang, Y., Sato, N., Zhang, S., ... Ma., Y. (2018). Conjugate Observations of the Evolution of Polar Cap Arcs in Both Hemispheres. *Journal of Geophysical Research*, *123*, 1794-1805. doi: 10.1002/2017JA024272

Acknowledgments

This work was supported by the Natural Environmental Research Council (NERC) studentship number NE/L002531/1. R.C.F. was supported by the United Kingdom's Science and Technology Facilities Council (STFC) Ernest Rutherford Fellowship ST/K004298/2. D.K.W, B.S.L. and J.M.C. are supported by NERC grant NE/N004051/1. D.J.P. was supported by the NERC studentship NE/R009783/1. The SSUSI data were obtained from http://ssusi.jhuapl.edu/. The DMSP particle detectors were designed by D. Hardy of Air Force Research Laboratory, and data were obtained from the Johns Hopkins University Applied Physics Laboratory. OMNI data were obtained from `https://omniweb.gsfc.nasa.gov/`. The authors acknowledge the use of SuperDARN data. SuperDARN is a collection of radars funded by the national scientific funding agencies of Australia, Canada, China, France, Italy, Japan, Norway, South Africa, UK, and United States. The raw SuperDARN data are freely available from the BAS SuperDARN data mirror (`https://www.bas.ac.uk/project/superdarn`). The ASK and HiTIES data used in this study are available at this website: `https://eprints.soton.ac.uk/439079/`. The Sony All Sky Camera data were provided by the Kjell Henriksen Observatory/The University Centre in Svalbard (UNIS).